Proceedings World Geothermal Congress 2020+1
Reykjavik, Iceland, April - October 2021

Multi-Dimensional Inversion of Electromagnetic Data from Alalobeda, Tendaho Geothermal Field in NE-Ethiopia and its Geothermal Significance

Getenesh Hailegiorgis Abebe[1, 3, 4], Gylfi Páll Hersir[2], Ásdís Benediktsdóttir[2], Halldór Geirsson[3]

[1]Geological Survey of Ethiopia, P.O. Box 2302, Addis Ababa, Ethiopia, [2]Iceland GeoSurvey (ÍSOR), Grensásvegur 9, 108 Reykjavik, Iceland, [3]University of Iceland, Sæmundargata 2, 101 Reykjavík, Iceland, [4]UNU-GTP, Orkustofnun, Grensásvegur 9, 108 Reykjavík, Iceland

getenesh19@gmail.com; abeb@unugtp.is

Keywords: Tendaho, Alalobeda, geothermal, resistivity structure, joint inversion, 3D inversion, joint interpretation

ABSTRACT

Tendaho is one of the high-temperature geothermal fields within the Main Ethiopian Rift (MER) in the Afar depression, NE-Ethiopia. It is located in one of the most important geothermal zones of the world. Due to its location and size, Tendaho is a promising area for geothermal development. Alalobeda is one of the three geothermal prospects in Tendaho, located on the southwest shoulder of Tendaho Graben. Detailed surface exploration studies were carried out jointly by the Geological Survey of Ethiopia (GSE) and ELC-Electroconsult in Italy financed by the Icelandic International Development Agency (ICEIDA) and the Nordic Development Fund (NDF). With financial support by ICEIDA/NDF in Alalobeda prospect recently including; gravity, micro-seismic and combined use of MT and TEM soundings. The main objective of the survey was to come up with a detailed resistivity model and image the deep resistivity structure, detect and characterise the possible geothermal reservoir of the Alalobeda geothermal prospect and propose drilling sites. The static shift correction of the MT data was made by jointly inverting the MT and TEM data from the same site. Joint 1D inversion of 108 MT/TEM sounding pairs and a 3D inversion of the off-diagonal impedance tensor of 107 MT soundings have been done.

The results of joint 1D inversion of MT/TEM and 3D inversion of the resistivity distribution from Alalobeda prospect gave comparable results at shallow depths. However, at a deeper level, 3D inversion reveals much more consistent details confirming that the resistivity structure in the area is highly three dimensional. From both inversion approaches, three main resistivity structures were observed. The first one is a thin layer of very low resistivity (< 10 Ωm) at shallow depth down to 300 m b.s.l, which is correlated with the sedimentary formation or smectite zone. The second layer is a resistive core between the depths of 1000 m to 4000 m b.s.l, which correlates with less resistive Afar Stratoid Series or the chloride-epidote zone. Beneath this resistive core, a deep conductor is imaged that could be associated with the heat source.

From the 1D and 3D approaches, lithological contacts and lineaments were identified. Sharp resistivity contacts or fault lines with an orientation of NE-SW transverse faults and NW-SE fault were observed. These identified faults and lineaments are in good agreement with gravimetric and micro-seismic results.

1. INTRODUCTION

The East African Rift System (EARS) is one of the areas in the world where numerous sites for harnessing potential geothermal energy are found. Most of the geothermal prospects in Ethiopia lie along the MER System. Among these is Tendaho, one of the geothermal fields in the MER System. Exploration of geothermal energy began in the MER in 1969 with a collaboration between the Ethiopian Government and United Nations Development Program (UNDP) (Bekele, 2012). Since then, about 23 geothermal prospects have been identified for direct use and electricity generation. However, most of the resources have not been explored and evaluated in detail. All the prospects are at different stages of exploration.

From 2014 to 2015 a detailed geoscientific exploration was conducted in Alalobeda geothermal prospect by Geological Survey of Ethiopia (GSE) and an Italian consulting company (ELC-Electroconsult) financed by Icelandic International Development Agency (ICEIDA) and Nordic Development Fund (NDF). A resistivity survey consisting of Magnetotellurics (MT) and Transient ElectroMagnetics (TEM) was a part of the project. A total of 132 co-located MT/TEM sounding data were collected and out of this 27 MT stations were collected in 2013 by GSE. The TEM data are used for static shift correction of the MT data from the same site.

The MT and TEM resistivity methods are currently the most widely used resistivity methods. Due to its ability to recover complex resistivity models of the subsurface of the Earth, three dimensional (3D) inversion of the MT data has become a common practice in geothermal exploration. Here, the objective is to get a detailed subsurface resistivity model and image the deep resistivity structure, delineate and characterize a possible geothermal reservoir of Alalobeda geothermal prospect and at the same time to compare different approaches of interpreting electromagnetic data, 1D and 3D, through the investigation of the resistivity structure of Alalobeda in order to infer the geothermal system therein and propose sites for exploratory/production drilling. A total of 108 MT stations are used in this work which is a part of the MS thesis work of the first author of this manuscript (Getenesh, 2019).

1.1 Location of Study Area

Tendaho is located 600 km northeast of the capital city, Addis Ababa, in the central Afar depression, where the three propagators join together (MER, Red Sea and the Gulf of Aden). Tendaho has undergone a number of geoscientific studies. In the Tendaho graben, there are three geothermal prospects, i.e. Dubti, Ayrobera and Alalobeda, as shown in

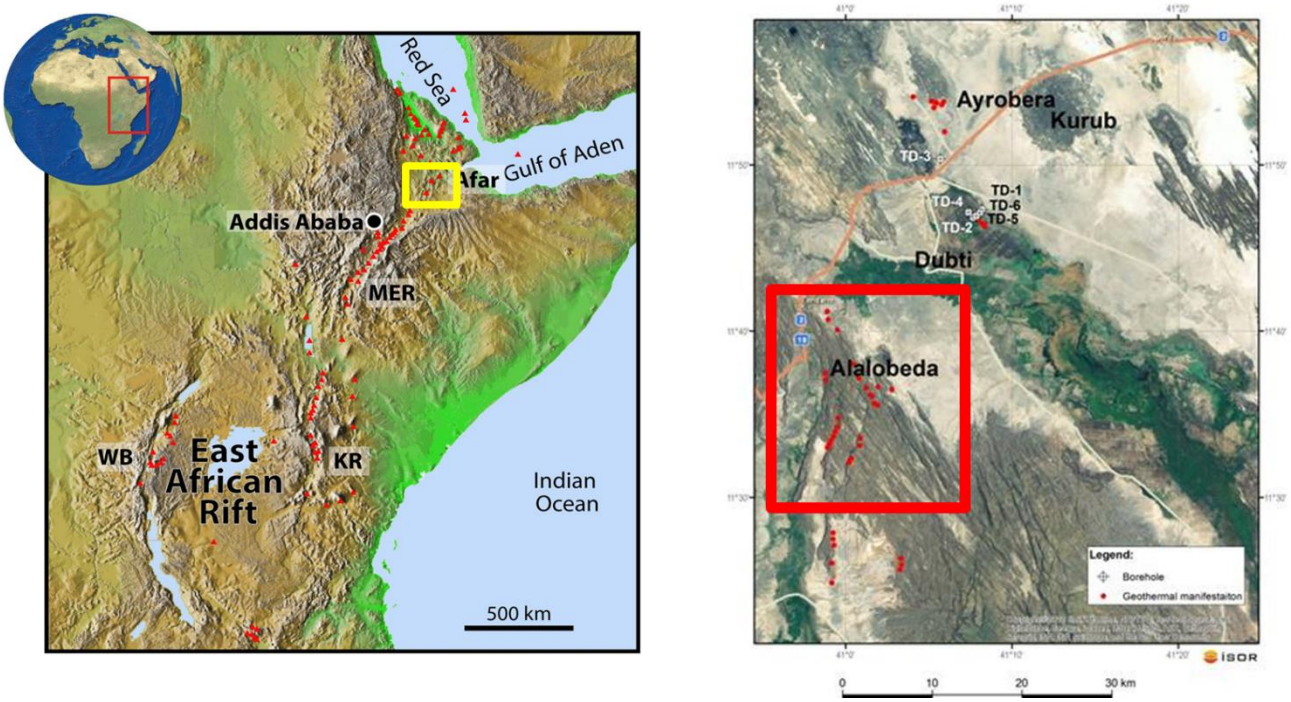

. Here, the area of interest is the Alalobeda geothermal prospect which is located in the western margin of the Tendaho graben. The Dubti and Ayrobera areas have undergone extensive geoscientific investigations. Deep exploratory wells have been drilled there. The drilled wells have proven the existence of a shallow reservoir of commercial interest in Dubti, whereas the deep reservoir appears to be characterised by an adequate temperature, associated with low permeability geological formation (Afar Stratoid basalt Series) (Aquater 1995, Aquater, 1996).

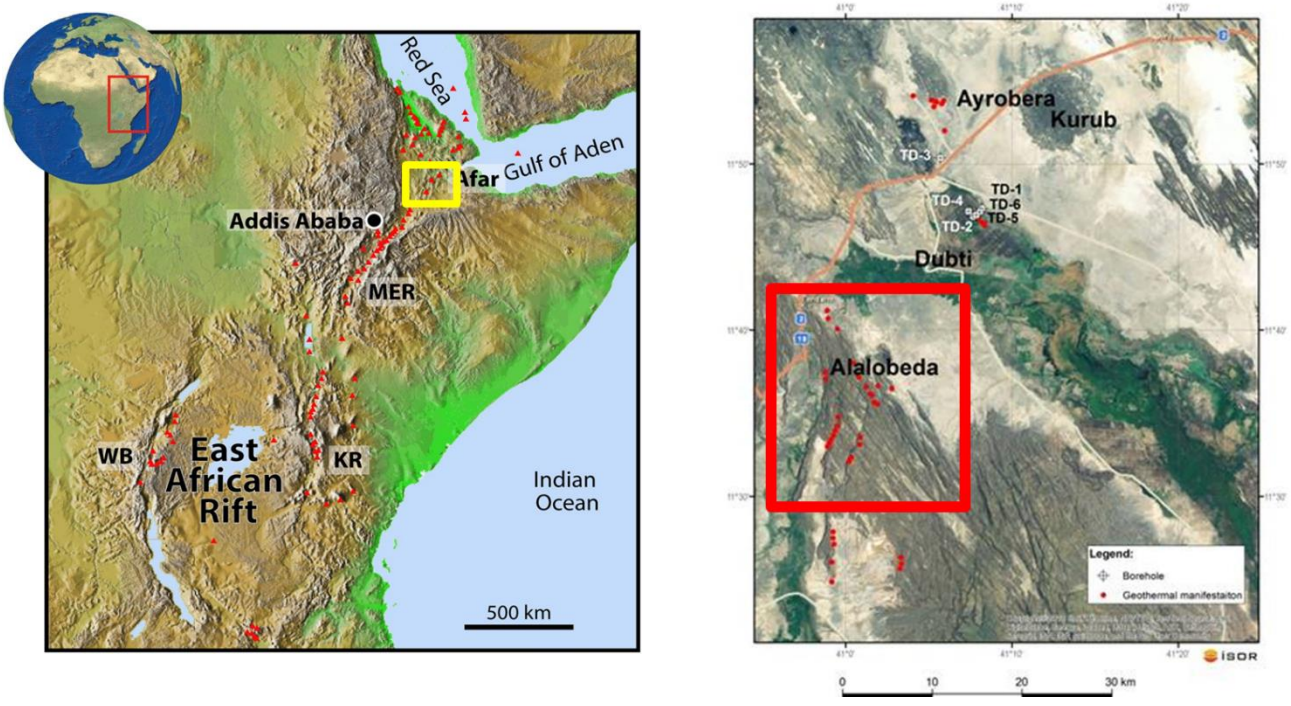

Figure 1: Left Figure shows the East African Rift. Main Ethiopian Rift (MER), Kenya Rift (KR), Western branch (WB). The yellow rectangle shows Tendaho geothermal field, right Figure an aerial photograph of Tendaho and the three geothermal fields. Red symbols and boreholes denote geothermal surface manifestations by white symbols. The red rectangle shows the study area.

2. PREVIOUS GEOTHERMAL WORK

2.1 Previous Geological Work

The northern part of the Tendaho rift is tectonically characterised by open fissures and active faults which define a pattern of NW-SE elongated blocks with a typical wavelength of some hundreds of meters. The northeast-trending Tendaho Graben, where the Alalobeda manifestations are located has a width of about 50 km and joins the Ethiopian Rift close to the Dama Ale volcano west of Lake Abhe. From a stratigraphic point of view, the youngest rocks of the regions are Quaternary axial fissural basalts and subordinate rhyolites and associated products and central volcanoes, the active historical volcano Kurub (younger products; 4,000 – 10,000 years) and Dama Ale (younger product; 2,500 years).

In the vicinity of the geothermal area in Tendaho, the most identifiable point of intersection is near Alalobeda, where NNE-SSW-trending faults of the MER terminate and deflect into the major NW-SE trend that bounds the graben on its southwest edge (Stimac et al., 2014)

A geological survey was conducted in Alalobeda prospect in 2015 through a collaboration between GSE and ELC: It led to the conclusion that Alalobeda has two distinct groups of rocks; (1) a ridge of Plio-Pleistocene age forming volcanic rocks and their minor intercalated sediments, (2) a rift floor dated from Pleistocene to present filling continental sediments intercalated with some lava flows (for more details, see ELC's geological report (ELC, 2015a)).

2.2 Previous Geochemical Work

The hot spring water from Alalobeda (Figure 1) and Bagalodoma are sodium chloride type with high sulphate contents. The Na, K, Mg diagram shows that the Alalobeda water has a trend towards full equilibrium (Aquater, 1996). A radon survey which was done by Teclu and Mekonen (2013) revealed the distribution of buried faults, joints and fractures. The investigation confirmed that the anomalous values are concentrated in the NNE/SSE and NS direction of the Alalobeda prospect. A recent geochemical report done by ELC (2015b) concluded that from the Na-K and K-Mg geothermometers of Giggenbach (1988) based on the samples from Alalobeda thermal spring (Figure 11) indicates a reservoir temperature of 220 °C. The Na-K and silica (quartz) geothermometers by Giggenbach et al. (1994) and Fournier (1973) indicate deep geothermal reservoir temperature close to 200 °C. From the ternary diagram, the Alalobeda water is chloride rich.

2.3 Previous Geophysical Work

In Tendaho, the first reconnaissance survey was done by UNDP and EIGS in 1973 (Megersa and Getaneh, 2006), to investigate deep structures and to delineate possible geothermal reservoirs. An MT survey was carried out in Afar in 1971, to investigate the electrical resistivity distribution (Berktold, 1975), which identified a layer with resistivity varying from 200-500 Ωm in the uppermost kilometre, to 5-10 m at about 15 km depth. A gravity survey was carried out by Aquater (1980) which revealed a -57 mgal gravity anomaly in Dubti plantation, which was attributed to thick sediments. A gravity survey carried out by ELC (2015c) inferred different lineaments and geological structures.

3. RESISTIVITY STRUCTURE OF HIGH GEOTHERMAL FIELDS

Geothermal systems are mostly found in regions, where there are elevated heat flow and structural settings that support vigorous fluid circulation through fractures. These regions are generally located along with major tectonic regimes and over mantle hot spots (Stimac, 2015).

The resistivity structure of high-temperature geothermal fields in the volcanic environment has been studied by several authors (Árnason et al., 1987; Árnason et al., 2000; Ussher, 2000; Flóvenz et al., 2012; Lévy et al., 2018). Generally speaking, a typical resistivity structure shows high resistivity in the uppermost part of the subsurface indicating cold or unaltered rocks, where the main conductive mechanism is pore fluid conduction. Below the high resistivity zone, a conductive cap is found consisting of conductive alteration minerals like smectite and zeolite with surface conduction mechanism. Below the conductive cap, the resistivity increases as a core of high resistivity appear. The transition from the conductive cap to the high resistive core coincides with a change in the mineral alteration from smectite to mixed-layered clay zone at a range of temperature 230-250 °C. At about 250 °C chlorite becomes more dominant. As the temperature increases to 250-270 °C, epidote becomes abundant. There, resistivity starts to increase again, because epidote has low cation exchange capacity making them more resistive (Árnason et al., 2000; Lévy, 2018). Figure 2 shows a schematic picture of the resistivity structure of a high-temperature geothermal area and its relationship with alteration minerals, temperature and conduction mechanism.

Therefore, resistivity is directly related to the alteration minerals but not necessarily related to present rock temperature. Because the geothermal system might not be active - could be fossil - resistivity reflects alteration that was formed in the past. Therefore, care must be taken when interpreting the resistivity structure and temperature.

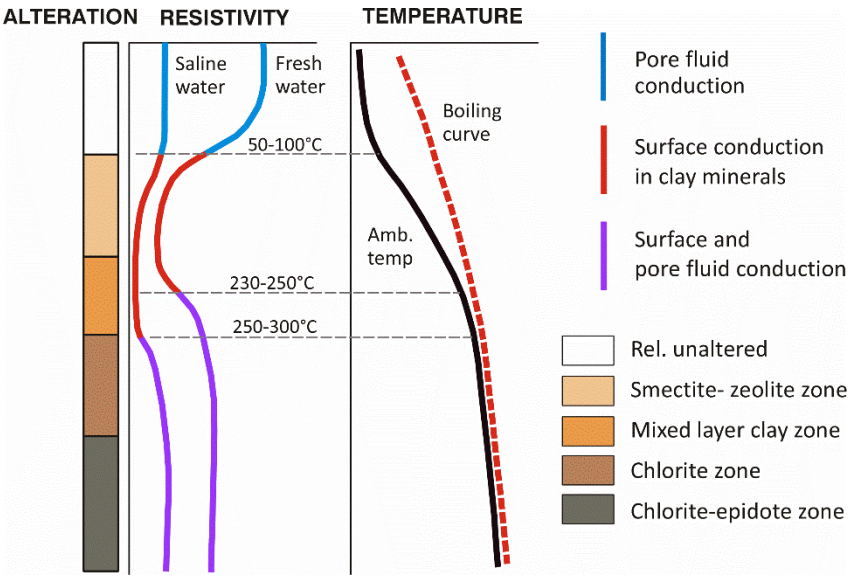

Figure 2: The general resistivity structure of a high-temperature geothermal system in basaltic environment showing resistivity variation and temperature (Flóvenz et al., 2012).

4. ELECTROMAGNETIC (EM) RESISTIVITY METHODS

EM resistivity methods are the most common geophysical method in surface exploration studies of geothermal areas, delineating the spatial distribution of the resistivity structure of the subsurface.

4.1 Magnetotelluric (MT) Method

MT is a passive EM exploration method that measures the fluctuations of the natural electric **E,** and magnetic **B**, fields in orthogonal directions on the surface of the Earth to determine the electrical properties of the Earth. The MT method is used for probing deep structures of the Earth´s subsurface from tens of meters to several tens of kilometres depending on the recording period and resistivity structure under the site (Flóvenz et al., 2012). There are two frequency ranges in MT data acquisition: high frequency (short period) which is used to detect shallow lying structures due to their short depth of penetration whereas low frequency (long period) is used to detect deep-lying structures of the Earth´s subsurface. The standard setup of an MT site is shown in Figure 3.

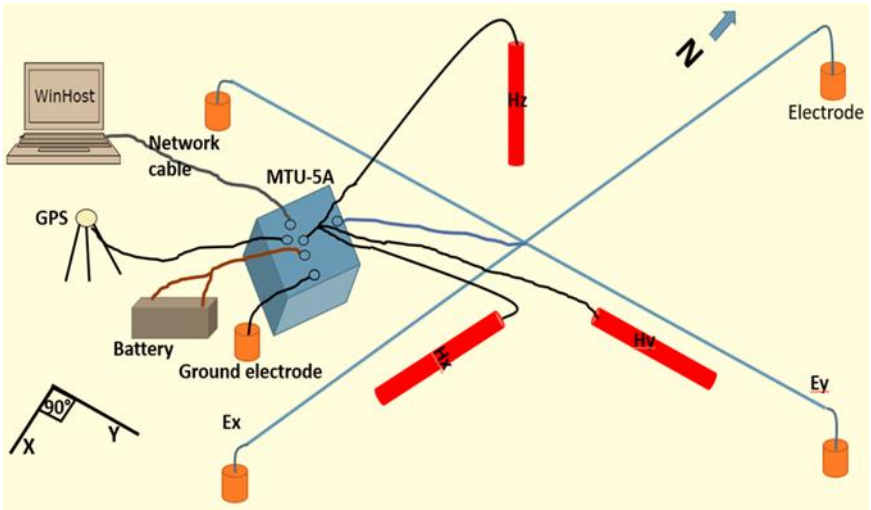

Figure 3: Standard set up of an MT site.

4.1.1 MT Survey and Instrumentation

The MT survey was carried out in Alalobeda in two field campaigns, in 2013 and 2014-15. An MT data acquisition system from Phoenix Geophysics Ltd Company in Canada (Phoenix Geophysics, 2009) was used for both field campaigns. In 2013, due to security problems at the survey site, the data were acquired only during the day time using two MTU-5A units. The instrument used for the MT survey consisted of a data logger (MTU), two pairs of electric dipoles for measuring the electric field, three induction coils connected by induction cables for measuring the time variations of natural magnetic field, battery, compact flash card, GPS and five non-polarizable electrodes, filled with lead chloride solution in a ceramic container that is designed to ensure good contact with the ground.

4.2 Transient Electromagnetic (TEM) Method

The Transient ElectroMagnetic (TEM) method is an active EM method, where the time-varying magnetic field is generated by a controlled artificial source (Árnason, 1989). In recent years the TEM method is becoming more common as a complementary tool to MT methods for investigating the deep structures of the subsurface.

A loop of wire laid on the ground and a constant magnetic field of known strength is built up by transmitting a constant current into the loop (Árnason, 1989) as shown to the right in Figure 4. The current in the source loop is abruptly turned off shown in the top left in Figure 4. Then the induced current is left without its source and responds by inducing an image of the source loop. This induced current dies out and generates a new secondary magnetic field that varies with time and as a result, induces new electrical current at greater depth in the ground. This new current density diffuses downwards and outwards into the ground and generates a new magnetic field decaying with time. The decay rate of the secondary magnetic field as a function of time is monitored by measuring the voltage induced in a receiver coil at the centre of the transmitter loop (Árnason, 1989) shown the left bottom of Figure 4. The decay rate of the secondary magnetic field and the current distribution depends on the resistivity structure of the Earth. The decay rate, recorded as a function of time after the current in the transmitter loop is turned off can, therefore, be interpreted in terms of the subsurface resistivity structure (Árnason, 1989; Flóvenz et al., 2012).

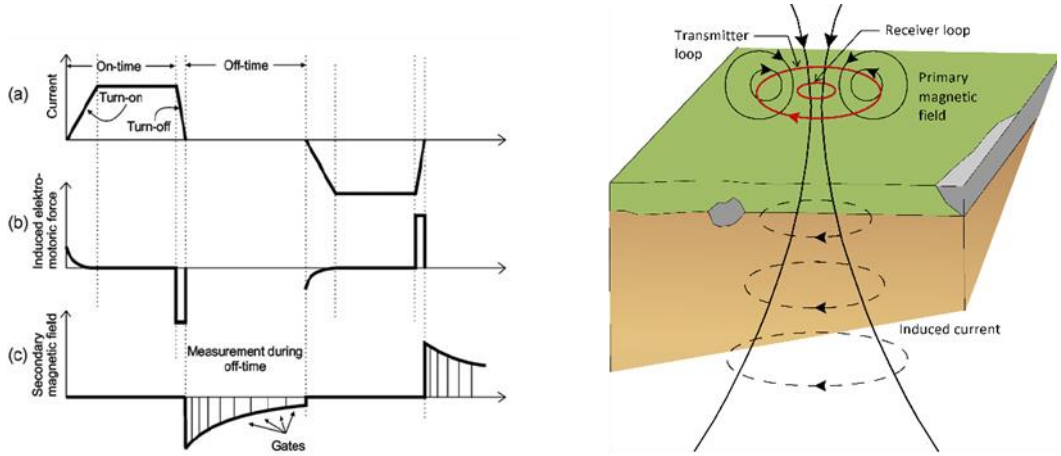

Figure 4: The right figure shows, the central loop TEM sounding configuration (Flóvenz et al., 2012; based on Hersir and Björnsson, 1991), the left figure shows, basic principles of the TEM method. (a) the current in the transmitter loop, (b) the induced electromotive force in the ground and (c) secondary magnetic field measured in the receiver coil (Christensen et al., 2006).

4.1.1 TEM Survey and Instrumentation

The TEM sounding data were acquired using two different instruments from two different manufacturers; Zonge GDP-32 and Phoenix V8 TEM systems. Both instruments consist of a transmitter, receiver coil with an effective area of 10000 m^2 (placed at the centre of the transmitter loop), transmitter loop, connecting cables, transmitter controller and power source. In most cases, the measurement was made using a 200 m x 200 m square transmitter loop and in some difficult terrain a 100 m x 100 m square.

5. DATA PROCESSING AND INVERSION

5.1 1-D Joint Inversion

In this study, 108 MT/TEM sounding data were 1-D inverted using a Linux-based program called TEMTD (Árnason, 2006). The inversion was done jointly for the TEM data and the rotationally invariant apparent resistivity and phase derived from the determinant value of the MT impedance tensor (see Flóvenz et al., 2012). The program determines the best static shift parameter for the MT data. An example of the joint 1-D Occam inversion of MT/TEM data is shown in Figure 5. The location of the soundings is shown in Figure 6.

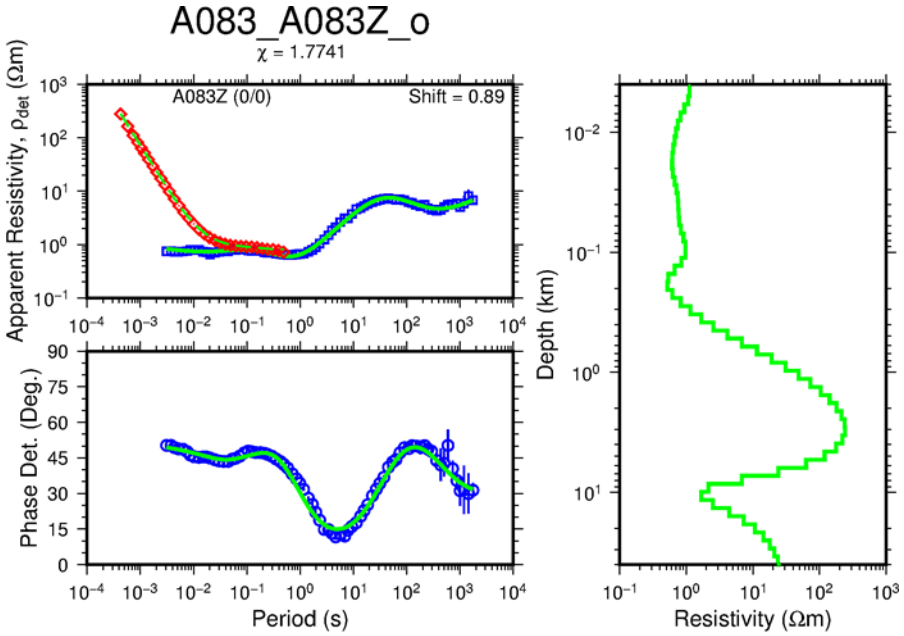

Figure 5: Result of joint 1-D inversion of MT and TEM soundings with TEM apparent resistivity (red diamond) transformed to a pseudo-MT cure, blue square and circle are measured apparent resistivity and phase respectively derived from the determinant of the MT impedance tensor; vertical blue lines error bars. Green lines show the response of the model calculation; on the right panel results of the 1-D resistivity model while on the left panel, its synthetic MT apparent resistivity and phase response. Number in parenthesis (0/0) indicates the two stations were at the same place, and the elevation difference was zero. The number on the top of the Figure, A083 name of MT station and A083Z name of TEM station. Static shift correction of 0.89.

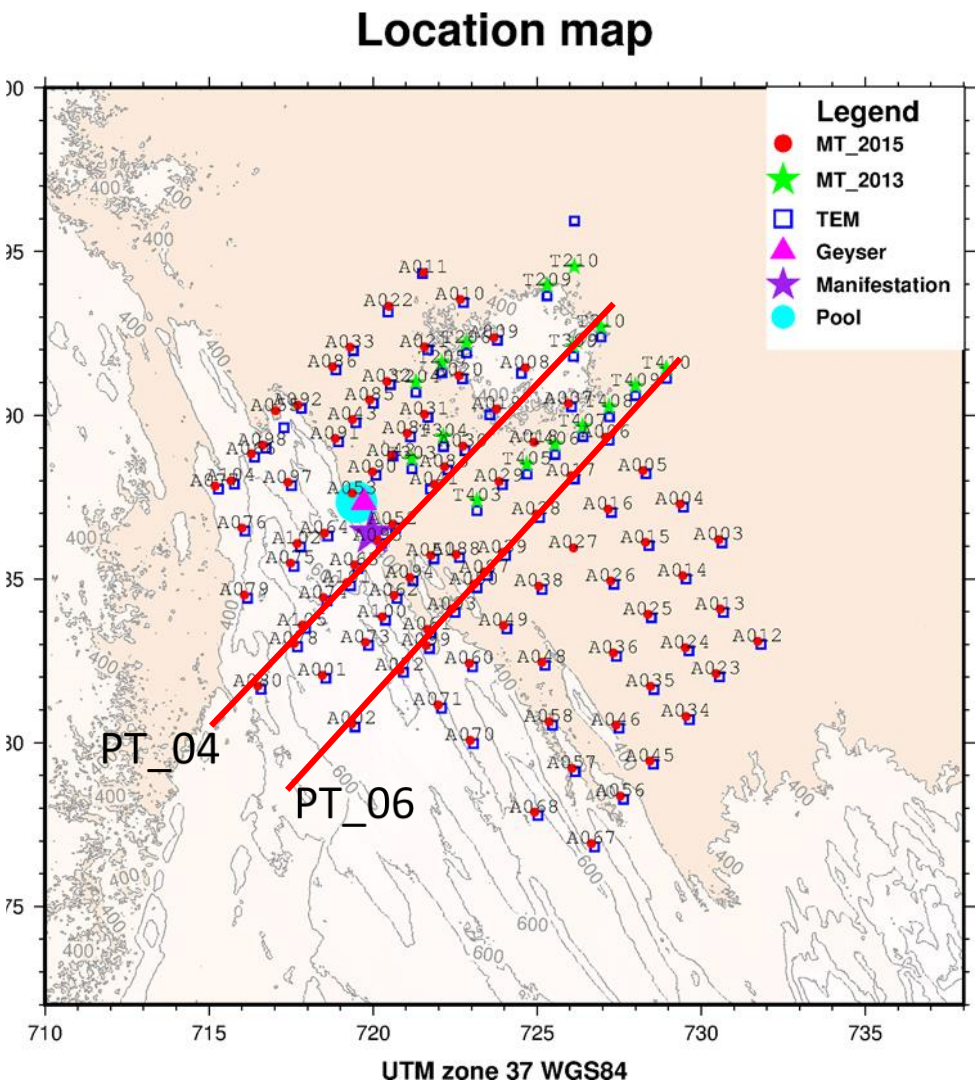

Figure 6: Location of MT and TEM soundings and resistivity cross-sections.

5.2 Static Shift Correction

MT data suffer from the static shift problem because of near-surface inhomogeneities that cause distortion of MT data due to an electric field generated from the boundary charges on surficial bodies and persist throughout the entire recording range of the MT sounding. To overcome this problem, all the MT sounding data were jointly inverted with TEM data acquired within a few meters from the same site. Figure 8 shows an example of a static shift correction of MT data. To the left in Figure 7, the histogram of the static shift parameters is shown, which is mostly in the range of 0.1 to 1.6 and the left Figure shows, the spatial distribution of the static shift map of the Alalobeda prospect is shown. From the map, we can see the apparent resistivity is shifted upwards in most of the area and downward in some of the areas due to near-surface inhomogeneities or topographic effect and also a small part of the area has not been affected by the static shift.

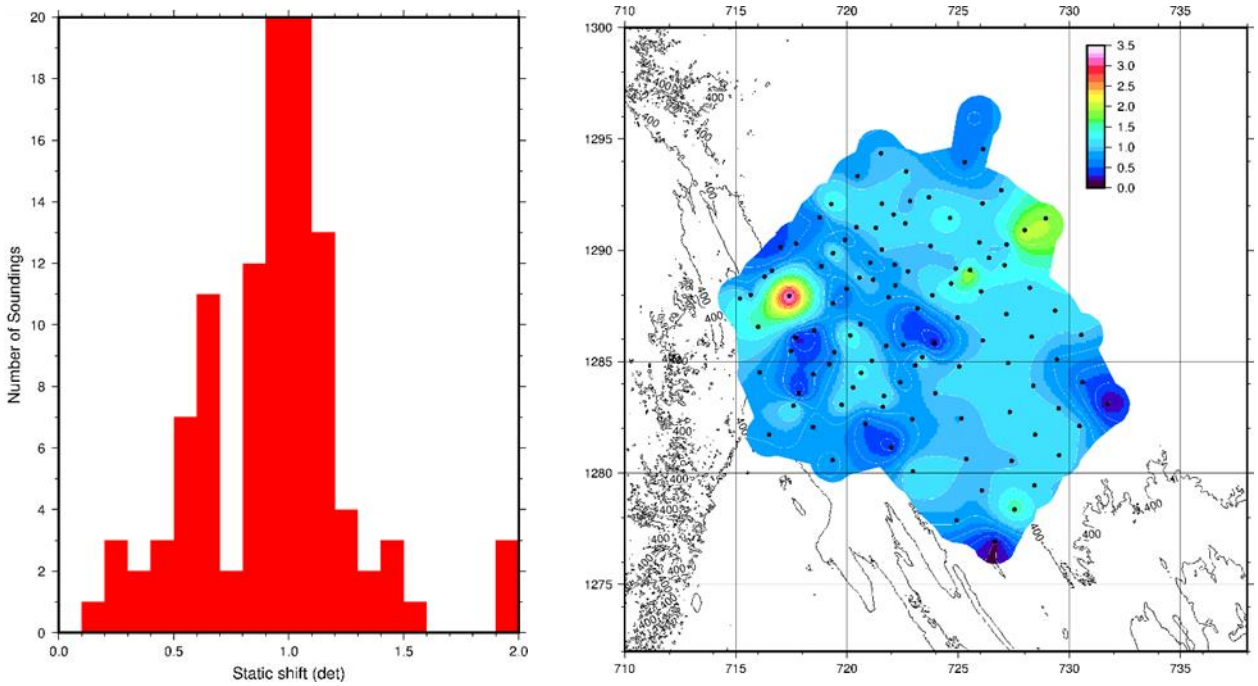

Figure 7: The Figure to the left shows a histogram of static shift parameters and the Figure to the right shows the spatial distribution of static shift parameters in Alalobeda prospect.

As mentioned above the MT curve is shifted up or down due to near-surface homogeneities or topographic effect. To the left in Figure 8, the Mt curve is shifted down, and the resistivity model gives wrong depth and resistivity structure; it gives shallow depth and low resistivity, for example, the first layer shows a depth of about 0.04 km and the resistivity is 0.3 Ωm and to the right in Figure 8, shows after the correction and the first layer shows a depth of 0.08 km and resistivity of 2 Ωm.

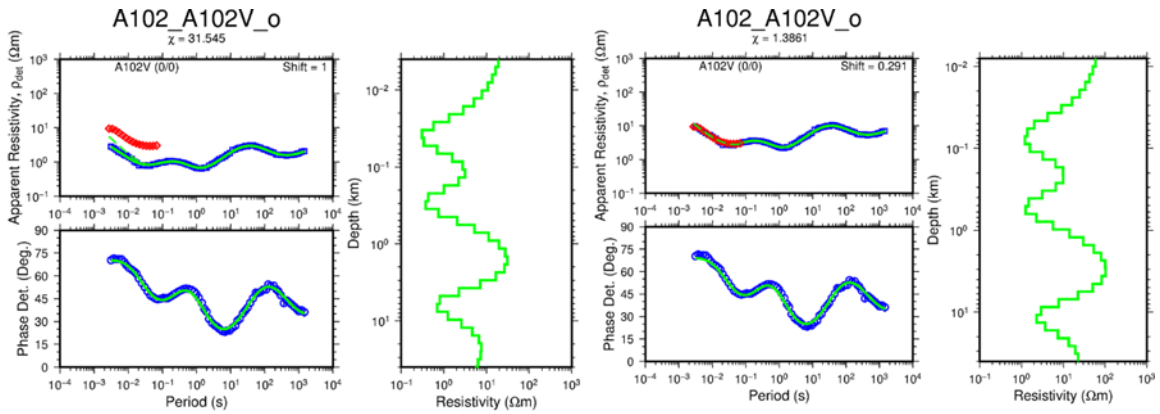

Figure 8: An example of static shift correction of MT data from Alalobeda prospect. The figure to the left shows before static shift correction and Figure to the right shows after static shift correction. For Figure legend, see Figure 5.

5.3 Results and Discussion of 1-D inversion

5.3.1 Pseudo-2D resistivity cross-sections

Pseudo-2D resistivity cross-sections were created based on the joint 1-D Occam inversion models of the MT and TEM data, using a Linux based program called TEMCROSS, which was developed at ÍSOR (Eysteinsson, 1998). Several cross-sections were made through the survey area, some of which were located perpendicular to the main geological structure. From the cross-sections, we can conclude that the resistivity structures are generally quite similar, with three main resistivity layers.

The uppermost part of cross-section PT_04 (Figure 9), is characterised by a thin layer of very low resistivity (<10 Ωm), associated with the sedimentary formation and possibly also influenced by smectite low-temperature alteration. The second layer is the high resistivity layer with a resistivity between varying between 100 and 1000 Ωm reaching down to a depth of 1000-4000 m b.s.l. associated with resistive Afar Stratoid basalt Series, possibly also influenced by high-temperature alteration minerals like chlorite and epidote. At greater depth resistivity decreases again <10 Ωm, which may indicate deep-lying conductor, related to the heat source.

The resistivity structure, i.e. up doming of the low resistivity around MT station A105 and between MT stations A052 and T309 may indicate an up-flow zone in the area.

Cross-section PT_06 shown in **Figure 10** has similar resistivity structure. The resistivity structure around MT station A087 and between MT stations A028 and T410 may indicate the up-flow zone in the area.

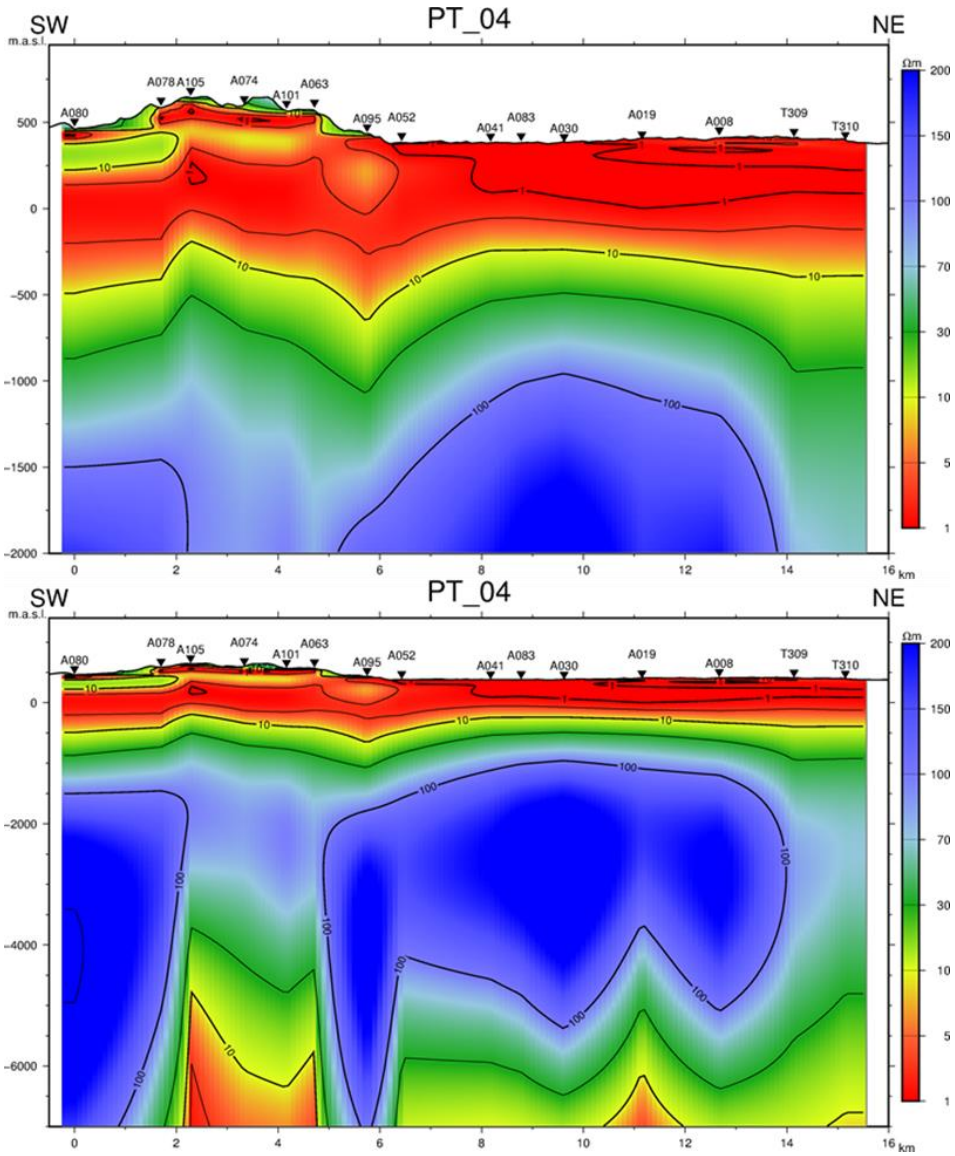

Figure 9: Resistivity cross-sections PT_04 down to a depth of 2000, and 7000 m b.s.l., for location see Figure 6.

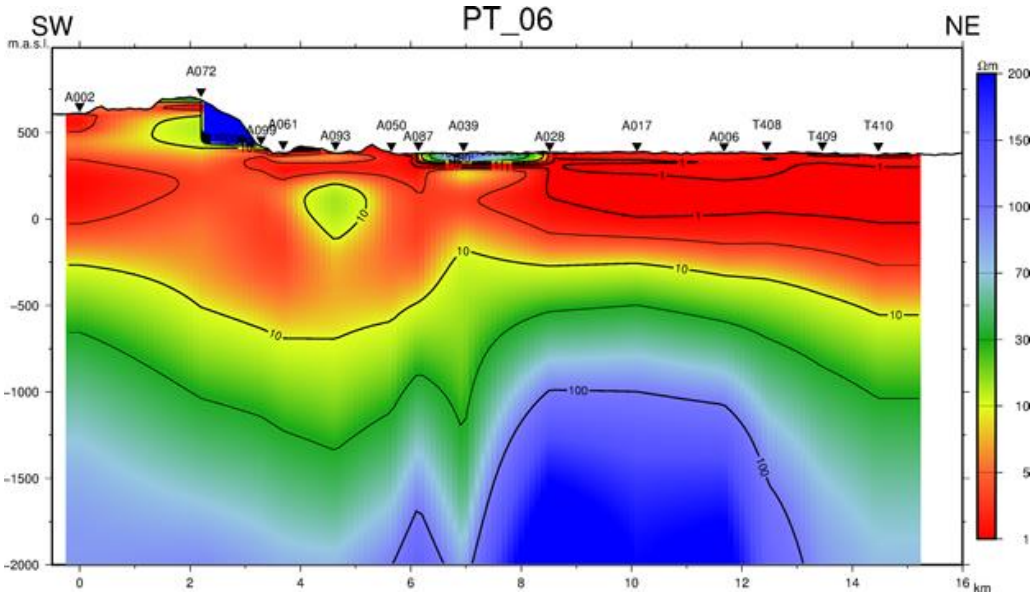

Figure 10: Resistivity cross-section for PT_06, for location, see Figure 6.

5.3.2 Resistivity depth slices

The program TEMRESD developed at ÍSOR (Eysteinsson, 1998) was used to plot the resistivity depth slices based on joint 1-D Occam inversion of MT and TEM data. Resistivity depth slices 300 m a.b.s.l and 800 m b.s.l are shown in Figure 11. At 300 m a.s.l., low resistivity is seen associated with sedimentary formation. At 800 m b.s.l., the resistive layer correlated with resistive Afar Stratoid basalt Series. However, along the NW-SE lying geological structure, the resistivity is still low at this depth, which may indicate the lateral flow of geothermal fluids along with the fractures and possibly also low-temperature alteration minerals like smectite.

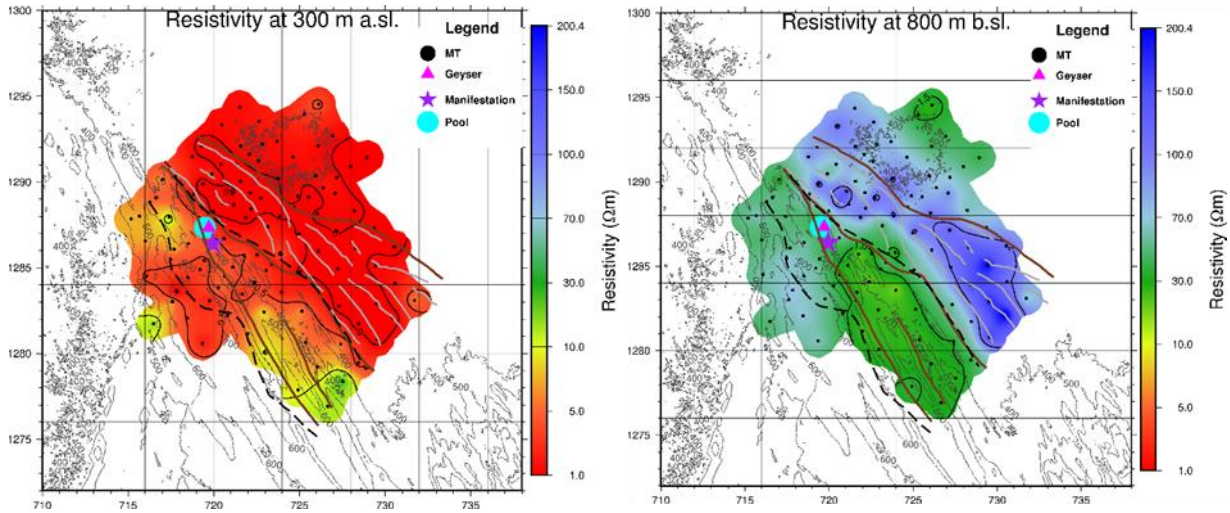

Figure 11: Resistivity depth slices from Alalobeda prospect based on Occam 1-Djoint inversion at 300 m a.s.l. and 800 m b.s.l. The grey line indicates the fault; white lines indicate lineaments inferred from gravity and broken black lines show the gravity low anomaly border.

6. 3-D INVERSION OF MT DATA

The 3D inversion was done using the inversion program written by Prof. Weerachai Siripunvaraporn (Siripunvaraporn et al., 2005; Siripunvarapornn and Egbert, 2009). The 3-D inversion is based on the model space matrices. The computation is dependent on the size of the model parameter M. To overcome the inversion problem, the 3-D inversion code WSINV3DMT uses finite different, forward algorithm and utilizes a formulation of the inverse problem in the data-space N rather than in the model space M. This approach reduces the dimensionality of the problem dramatically and makes the 3-D inversion of the MT data attainable. For this study the total size of the data values was 12,960 (i.e. $N=N_s*N_r*N_p$), where, Ns is the total number of station used for the inversion (108 soundings), Nr number of response, in our case it is 4 because we only used the off-diagonal impedance tensor components (2 real and 2 imaginary) and Np, the total number of period we used 30. On the other hand, the model parameter is 110.592 (i.e. M = x*y*z), where the grid cells were 64, 64 and 27, in the x, y and z-direction, respectively.

6.1 Data Preparation

To get a reasonable resistivity model, we exclude the noisy stations and MT stations that do not have the corresponding TEM stations. The MT stations used in the 3-D inversion were those that had less noise and with longer period data points and they are evenly distributed over the survey area.

The computational intensity of the inversion is directly proportional to the number of periods that we used for the inversion. Therefore, in order to reduce the computational cost (time and memory), the static shift corrected impedance tensor was resampled at 30 periods, equally spaced on the log scale. In this case, five data periods per decade were selected in the range of 0.0032 s to 700 s, which will give enough resolution to get detailed resistivity structure. Resampling the data is not only to reduce the size but also makes the data smoother. After resampling, we prepared skip list from the resampled data by skipping the noisy data points, and the noisy data points are excluded in the inversion.

6.1.1 Static Shift Correction

The 3-D inversion was performed for the MT impedance tensor components that may contain static shifts. Therefore, static shift correction was needed for the MT impedance tensor components. It is assumed that the static shift is dominantly due to the distortion of the electric field. The impedance tensor static shift correction can be done using the following equation.

$$\begin{bmatrix} Z_{xx}^{c} & Z_{xy}^{c} \\ Z_{yx}^{c} & Z_{yy}^{c} \end{bmatrix} = \begin{bmatrix} C_x & 0 \\ 0 & C_y \end{bmatrix} \begin{bmatrix} Z_{xx} & Z_{xy} \\ Z_{yx} & Z_{yy} \end{bmatrix};\ C_x = \sqrt{\frac{1}{S_{xy}}};\ C_y = \sqrt{\frac{1}{S_{yx}}} \tag{1}$$

where Z^c is the corrected and Z the uncorrected impedance tensor, S_{xy} and S_{yx} are shift multiplier of the xy and yx apparent resistivity respectively.

All un-rotated MT data were jointly inverted with the TEM data from the same location, for both xy and yx modes and the shift multiplier parameters S_{xy} and S_{yx} were determined.

6.2 Model Grid

The mesh grid consists of 64 vertical grid cells in the x-direction (two edges and 62 internal cells), 64 vertical grid cells in the y-direction (two edges and 62 internal cells) and 27 horizontal grid cells in the z-direction (one surface, one bottom and 25 horizontal internal cells). The grid design was made by considering the area of interest and data coverage. The grid is denser in the area of interest and the area of the data coverage with 400 m grid spacing.

6.3 Initial Models

To investigate the influence of the initial model on the results, two different initial models were applied.

(1) Model compiled from joint 1D inversion of MT/TEM sounding pairs hereafter referred to as the J1D model

(2) A homogeneous half-space with resistivity 10 Ωm. Hereafter referred to as H010 model.

We were also testing 50 Ωm and 30 Ωm the inversion could not converge. The inversion was done using a Linux-based program using the WSINV3DMT code. It was executed on 32 core computer with 132 GB memory. The procedure used in the inversion was to run the inversion for at least five iterations at each step which is then restarted with the best model for the next run.

6.4 Result and Discussion of the 3-D inversion

The 3D program assumes a flat surface. The MT data were static shift corrected prior to the inversion which somewhat removes the topographic effects in the data. The resistivity models resulting from the 3D inversion were elevation corrected (since the program assumes flat surface we did elevation correction after getting the 3D results) and the results are presented as smoothed resistivity maps at different elevations and as resistivity cross-sections. We choose the result from the J1D initial model because the H010 doesn't resolve the deep structure.

6.4.1 Resistivity Depth Slices

In the fine grid, there are some areas where there are no data points. Artefacts are prone to appear in these areas, and this should be noted when the 3D model is being looked at. An example of an elevation corrected resistivity depth slice at 200 m a.s.l. is shown in Figure 12. Here, the map shows most of the flat area indicates very low resistivity which is associated with sedimentary formations, but along the main geological structure a circular shape of around 30 Ωm is seen maybe associated unaltered or permeable Afar Stratoid basalt.

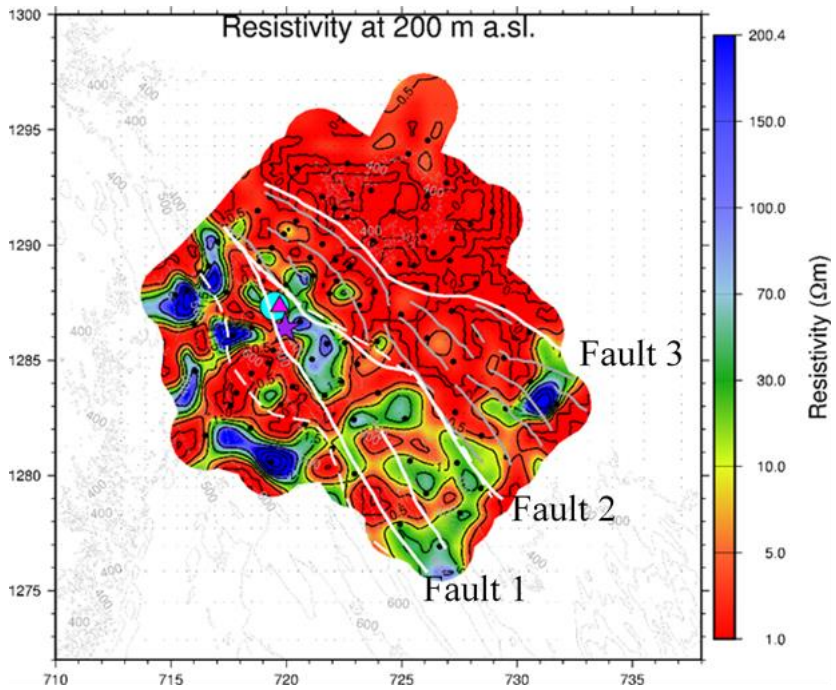

Figure 12: Resistivity depth-slice at 200 m a.s.l. based on an initial J1D model. The white line indicates the fault; the broken white lines show the gravity low anomaly border; grey lines indicate lineaments inferred from gravity. For the other legend, see Figure 11.

6.4.2 Resistivity Cross-Section

Smoothed elevation corrected resistivity cross-sections based on the inversion using J1D initial model is given in Figure 13 and Figure 14. It shows mostly three resistivity layers as described in the result on the 1-D joint inversion.

The 3-D result gives a more detail resistivity structure, from Figure 13, three resistivity layers are revealed; a well-defined high resistivity core appears below the low resistivity cap.

Figure 13 shows a vertical resistivity cross-section, NS_E-3800. It passes perpendicular through the three main faults in the survey area. This cross-section is characterised by a thin layer of very low resistivity, < 10 Ωm, with a varying depth from sea level down to 200 m b.s.l. The layer is most likely associated with the shallow sedimentary formation. Below the low resistivity, a high resistivity layer is found with resistivity values around 100 Ωm and even more down to depths varying between 1200 and 4000 m from the surface. The high resistivity could be related to the high resistive Afar Stratoid basalt series. The shallow-lying high-resistivity anomaly observed below stations A053, A073 and A090 could be the high resistive Afar Stratoid basalt intercalated with the sediment. A low-resistivity column is observed at around x=-4, and it could be an up-flow zone as it lies close to Fault 1 and the surface manifestations. The other plausible up-flow zone is seen close to station A063 through Fault 2 around 0 in the x-axis.

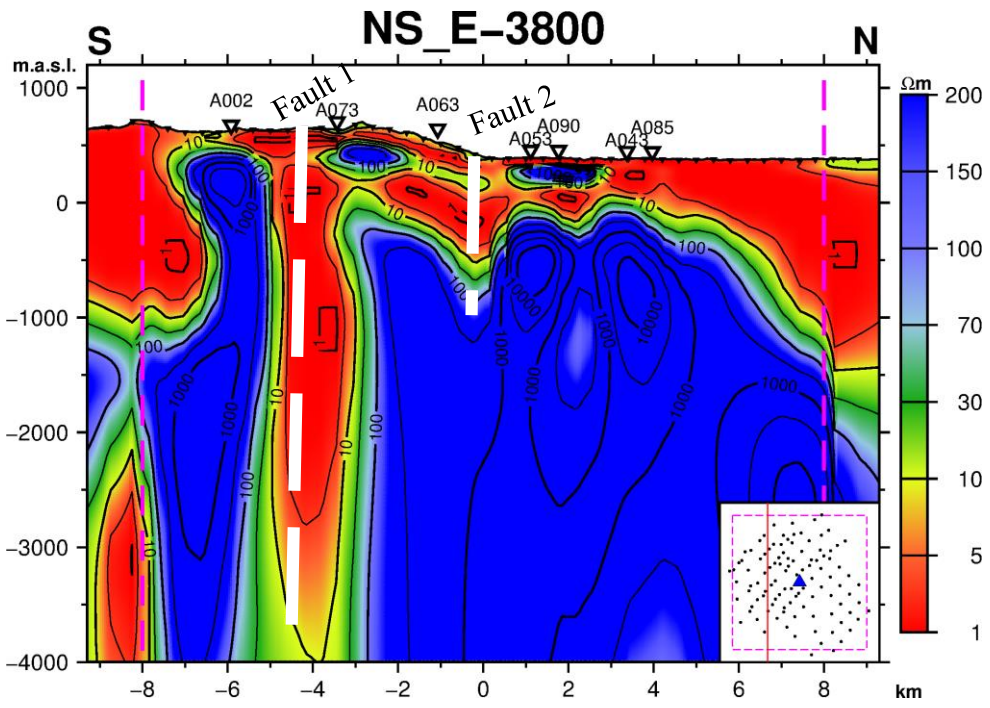

Figure 13: Resistivity cross-sections NS_E-3800. Name of the MT stations are given on top, the location of the cross-section is in the right corner, and broken pink lines show the extent of the fine grid.

Figure 14 shows a resistivity cross-section, NS_E1400. It shows a similar resistivity structure, as mentioned before. The three plausible up-flow zones are at x=-5, x=-1 and x=+4 and correspond to faults 1, 2 and 3, respectively. It seems that fault 2 and 3 might have a common up-flow from depth in this area, here seen at +2 in the x-axis. This may also indicate that their heat source is the same

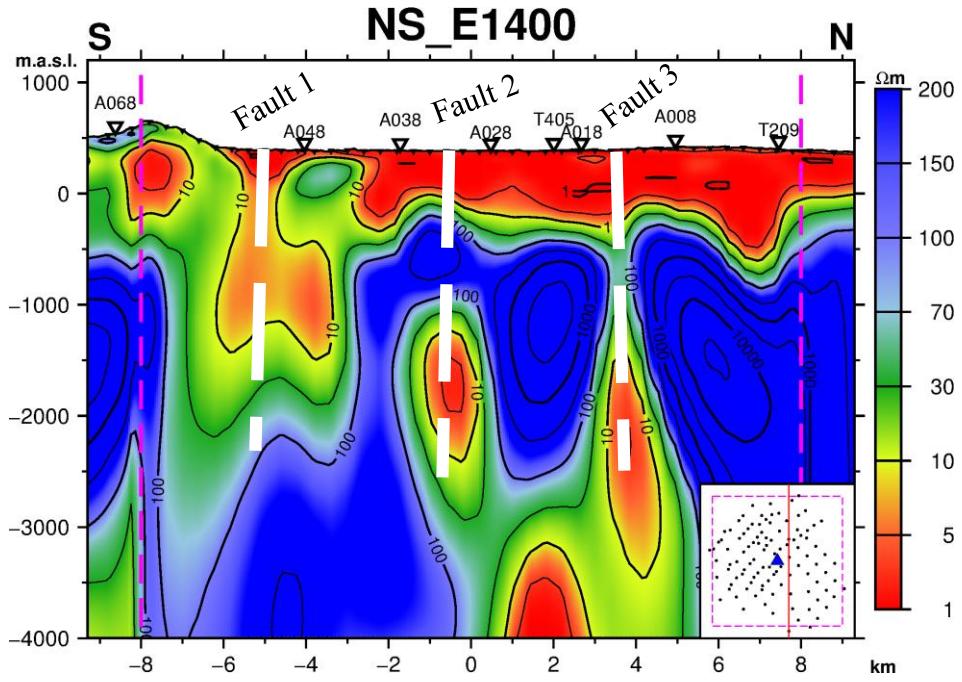

Figure 14: Resistivity cross-sections NS_E-3800. Name of the MT stations are given on top, the location of the cross-section is in the right corner, and broken pink lines show the extent of the fine grid.

7. COMPARISON OF THE 1-D AND 3-D RESULTS

The 3-D inversion results of the MT data show more or less a similar resistivity distribution at a shallower depth. However, at deeper level, 3D inversion reveals much more consistent details confirming that the resistivity structure in the area is highly three

dimensional. At 100 m b.s.l. Figure 15a and Figure 15b models from the J1D (3D) and joint 1D Occam inversion respectively: both maps show generally low resistivity, but the 3-D shows more detailed resistivity structure in the area.

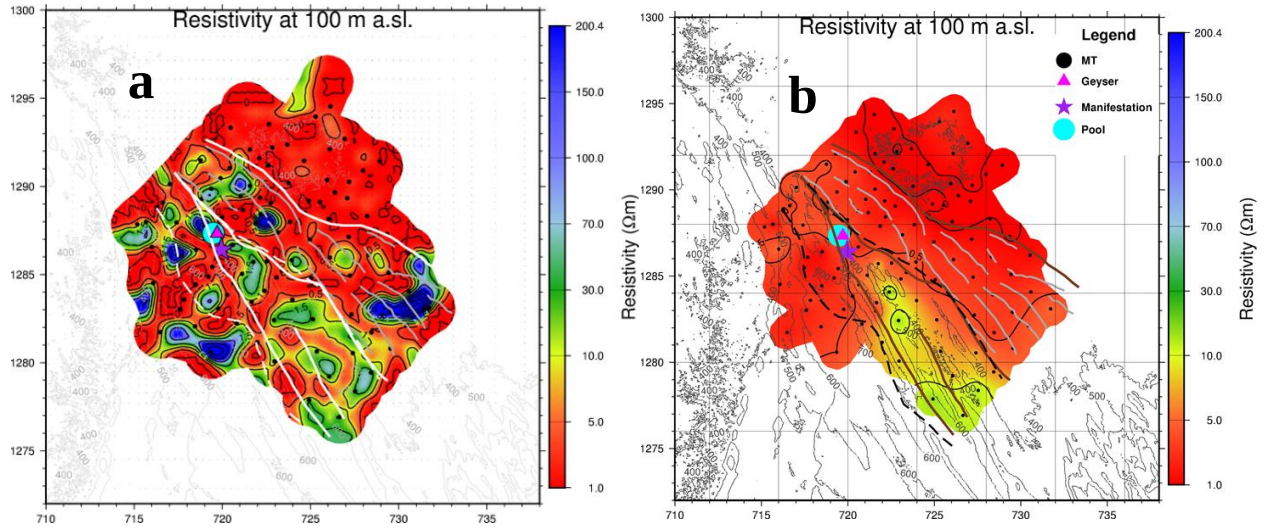

Figure 15: Comparison of 3D and 1D depth-slices map at 100 m a.s.l. (a) The 3D inversion from J1D model (b) joint 1D Occam inversion. For Figure legend, see Figure 12.

At 5000 m b.s.l. Figure 16a and Figure 16b models from the J1D (3D) and joint 1D Occam inversion respectively: most of the area is characterised by low-resistivity. At this depth, the resolution of the MT data has diminished greatly. The low-resistivity layer at depth could be a heat source

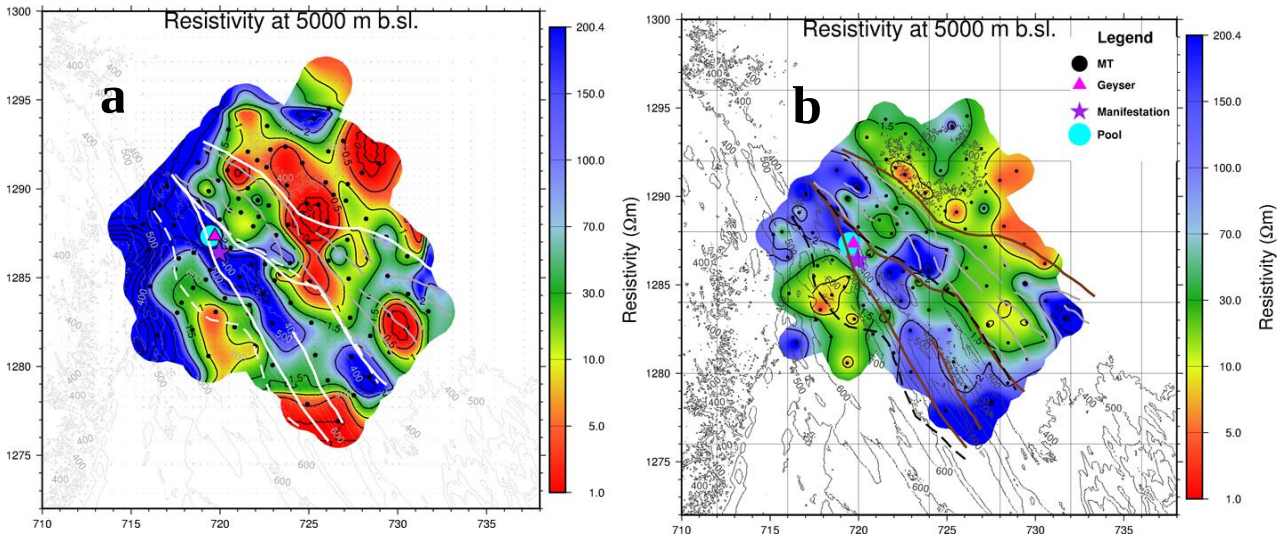

Figure 16: Comparison of 1D and 3D depth-slices map at 5000 m b.s.l. (a) The J1D model, (b) joint 1D Occam inversion. For Figure legend, see Figure 12.

8. CONCLUSIONS

Multi-dimensional inversion was done for a total of 108 MT and TEM sounding data. The 3D inversion was performed for the off-diagonal impedance tensor elements and 30 periods logarithmically distributed on the log scale were used. Two initial models were run:

- a model compiled from the Occam 1D joint inversion and
- a homogenous half-space of 10 Ωm resistivity.

The results of 1D joint inversion of MT/TEM data and 3D inversion gave comparable results at shallow depths. However, at a deeper level, 3D inversion reveals much more consistent details confirming that the resistivity structure in the area is highly three dimensional.

The resistivity structure of the Alalobeda prospect generally has three resistivity layers. At shallow depth, there is a thin layer around 1000 m below the surface with varying depth with low resistivity <10 Ωm associated with the sedimentary formation or low-temperature alteration mineral-like smectite. The second layer 1100 m to 4000 m from the surface with varying depth shows high resistivity>200 Ωm which may be associated with the resistive Afar Stratoid basalt Series or high-temperature alteration minerals like chlorite and epidote. At greater depth (around 4500 m from the surface) the deep-lying conductor is revealed which could be associated with the geothermal heat source.

A few prominent vertical low resistivity anomalies are seen in the vertical cross-sections extending from the resistivity at shallow depth down to even 5 km depth. It turns out that these vertical anomalies follow the main NW-SE fault in the area. The most plausible explanation to this is that these anomalies show the pattern of the geothermal fluid along the faults from depth up to the sedimentary layers. The pathway may contain smectite, but the low resistivity may also be caused by the high temperature of the geothermal fluid and or salinity. An example of this is shown in Figure 13 and Figure 14 as resistivity cross-sections through the area

The 1-D and 3-D modelling results show resistivity discontinuities that have confirmed faults and lineaments inferred by gravity.

REFERENCES

Aquater, 1980: *Geothermal resource exploration project Tendho area feasibility study-Phase II*. EIGS and ministry of Foreign Affairs of Italy, San Lorenzo in Campo, report, (1980).

Aquater: *Tendaho geothermal project, final report*. MME, EIGS, Government of Italy, Ministry of Foreign Affairs, San Lorenzo in Campo, report, (1996).

Árnason, K., Flóvenz, Ó.G., Hersir, G.P.: Resistivity structure of high temperature geothermal system in Iceland. International Union of Geodesy and Geophysics (IUGG) XIX General Assembly. Vancouver, Canada, Abstract V, (1987), 477p

Árnason, K.: *Central loop transient sounding over a horizontally layered earth*. Orkustofnun, Reykjavik, report OS-89032/JHD-06, (1989), 129pp.

Árnason, K., Karlsdóttir, R., Eysteinsson, H., Flóvenz, Ó.G., and Gudlaugsson, S.Th., 2000: The resistivity strcture of high-temperature geothermal systems in Iceland. *Proceedigs of the World Geothermal Congress 2000, Kyushu-Tohoku, Japan*, 923-928.

Bekele, B.: Review and reinterpretation of geophysical data of Tendaho geothermal field. GSE, Addis Ababa, unpublished report, (2012), 96pp.

Berktold, A.: Magneto-telluric measurements in the Afar area. Afar Depression of Ethiopia. *Proceeding of the International Symposium on the Afar Region and Related Rift Problems, Schweizerbart, I, Stuttgart*, (1975), 262-275.

Christensen, A., Auken, E., and Sorensen, K.: The Transient electromagnetic method. *Ground water Geophysics, **71***, (2006), 179-225.

ELC: Consultancy Services for Geothermal Surface Exploration in Tendaho Alalobeda, Ethiopia. Geological report, (2015).

ELC: Consultancy Services for Geothermal Surface Exploration in Tendaho Alalobeda, Ethiopia. Geochemical report, (2015).

ELC: Consultancy Services for Geothermal Surface Exploration in Tendaho Alalobeda, Ethiopia. Gravimetric report, (2015).

Eysteinsson, H.: TEMRESD, TEMMAP and TEMCROSS plotting programs. ÍSOR – Iceland Geosurvey, unpublished programs and manuals, (1998).

Fournier, R.O.: Silica in thermal waters: laboratory and field investigations. Proc. Int. 1 Symp. Hydrogeochemistry and Biogeochemistry, Tokyo, (1973), 122-139.

Flóvenz, Ó.G., Hersir, G.P., Sæmundsson, K., Ármannsson, H., and Fridriksson, Th.: Geothermal energy exploration techniques. In: Sayigh, A. (ed.), *Comprehensive Renewable Energy, 7*. Elsevier, Oxford, UK, (2012), 51-95.

Giggenbach, W.F.: Geothermal solute equilibria. Derivation of Na-K-Mg-Cl geoindicators. *Geochem. Cosmochim. Acta* **52**, (1988), 2749-2765.

Giggenbach, W.F., Sheppard, D.S., Robinson B.W., Stewart M.K., Lyon G.L.: Geochemical structure and position of the Waiotapu geothermal field, New Zealand. *Geothermics* **23**, (1994), 599-644.

Hailegiorgis,G., 2019: Multi-dimensional Inversion of Electromagnetic Data from Alalobeda, Tendaho Geothermal Field in NE-Ethiopia and its Geothermal Significance.

Hersir, G.P., and Björnsson, A., 1991: *Geophysical exploration for geothermal resources. Principles and applications*. NUN-GTP, Iceland, report 15, 94pp.

Hersir, G.P, Árnason, K., Villhjálmsson, A.M.: Krýsuvík high temperature geothermal area in SW Iceland: Geological setting and 3D inversion of magnetotelluric (MT) resistivity data. Journal of volcanology and Geothermal Research, (2018).

Megersa, G., Getaneh, E.: *Geological surface hydrothermal alteration geothermal mapping of Dubti-Semera, area, Tendaho geothermal field*. GSE, Addis Ababa, unpubl. report, (2006), 66pp.

Phoenix Geophysics: *V5 System 2000 MTU/MTU-A User Guid*. Phoenix Geophysics, (2009), 178p.

Siripunvaraporn, W., Egbert, G., Lenbury, Y., Uyeshima, M.: Three- dimensional Magnetotelluric inversion:data-space method. Phys Earth Plan Int. **150**, (2005), 3-14.

Siripunvaraporn, W., and Egbert, G.: WSINV3DMT: Vertical mangetic field transfer function inversion and Parallel implementation. *Phy. Earth Planet. Int.* ***173***, (2009), 317-329.

Stimac, J., Armadillo, E., Rizzello, D., Mandeno, E.: *Geothermal resource assessment of the Tendaho area*. Completed for UNEP and the Geological Survey of Ethiopia. (2014), 83pp.

Teclu, A., and Mekonen, M.: *Preliminary radon soil geochemical survey at Alalobeda geothermal prospect (Tendaho geothermal field).* GSE, GREAD, Addis Ababa, unpubl.report, (2013), 55pp.

Ussher, G., Harvey, C., Johnstone, R., Anderson, E.: Understanding the Resistivities Observed in geothermal Systems. In: Proceedings of the 2000 World geothermal Congress, Kyushu-Tohoku, Japan, May 28–June 10, (2000), 1915-1920.